



# Time Response of Natural Convection of Nanofluid CuO-H<sub>2</sub>O in Enclosure Submitted to a Sinusoidal Thermal Boundary Condition

M. Bouhalleb<sup>1†</sup> and H. Abbassi<sup>2</sup>

<sup>1</sup>*Unit of Computational Fluid Dynamics and Transfer Phenomena*

<sup>2</sup>*National Engineering School of Sfax, BP1173, 3038 sfax, University of Sfax, TUNISIA*

†Corresponding Author Email: [meftehbouhalleb@gmail.com](mailto:meftehbouhalleb@gmail.com)

(Received November 15, 2014; accepted June 4, 2015)

## ABSTRACT

A two-dimensional steady laminar natural convection in rectangular enclosure filled with CuO-water nanofluid is numerically investigated. The horizontal walls are thermally insulated and the left vertical side one is heated by a temporal sinusoidal temperature variation, whereas the right wall is kept at cold temperature. Mass Conservation, momentum, and energy equations are numerically solved by the finite volume element method using the SIMPLER algorithm for pressure-velocity coupling. This study has been carried out for four parameters: the volumetric fraction of nanoparticles  $\phi$  ( $0\% \leq \phi \leq 4\%$ ), aspect ratio  $Ar$  ( $0.25 \leq Ar \leq 1$ ), amplitude of temperature  $a$  ( $0.2 \leq a \leq 0.8$ ) and its period ( $0.2 \leq \theta \leq 0.8$ ). These simulations are performed at constant Rayleigh and Prandtl numbers ( $Ra=10^5$  and  $Pr=7.02$ ). Numerical results show that the addition of nanoparticles into the basic fluid has a double role, increasing heat transfer and reducing the response time of the system. The decreasing of aspect ratio shows an increasing trend of the heat transfer and increases the amplitude of Nusselt number. We also see that after a time period the system does not return to its initial state (hysteresis phenomenon) because of the system inertia.

**Keywords:** Nanofluid; Nanoparticles; Time response; Aspect ratio; Period.

## 1. INTRODUCTION

Natural-convection flows generated by buoyancy forces in rectangular closed cavities have been the subject of numerous studies in the past. Actually, considerable efforts are still devoted in the area, where this basic geometry remains still attractive. The interest in such problems stems from their importance in many engineering applications such as convective heat loss from solar collectors, thermal design of buildings, air conditioning, and recently, the cooling of electronic components and many other applications. In fact, in practical applications involving natural convection as a removal heat transfer mechanism, the energy provided to the system is variable in time and gives rise to unsteady natural convection flow. Solar collectors and printed circuit boards are examples of such systems submitted to variable thermal boundary conditions. Moreover, by an appropriate choice of the parameters characterizing the variable excitation (amplitude and period of a periodic heating or cooling temperature, for example), it becomes possible to establish a variety of dynamical regimes (periodic, quasi-periodic, intermittent, chaotic etc.) instead of a stationary

regime. In an earlier investigation, Lage and Bejan (1993) numerically and theoretically studied the problem of natural convection in enclosures with one side heated with a pulsating heat flux. They showed that the buoyancy-induced flow resonates to a certain frequency of the pulsating heat input and the resonance phenomenon is characterized by maximum fluctuations observed in the heat transfer evolution with the time-depending temperature period. M. Kazmierczak and Z. Chinoda 1992 studied the unsteady

Buoyancy-driven flow in an enclosure with time periodic boundary conditions, they showed that increasing the amplitude or the period of the hot wall temperature oscillation increased the cycle-averaged heat transfer only slightly.

Douamna *et al.* (2000) have studied numerically the two-dimensional natural convection in a horizontal channel heated from below with a temperature varying sinusoidally with time and provided with rectangular adiabatic blocks distributed on its lower wall. They showed that the three different routes leading to chaos were identified by progressively varying the amplitude and the heating variable temperature period.

Antohe and Lage (1996) theoretically and numerically investigated the case of clear fluid and fully saturated porous medium differentially heated enclosures with a time periodic pulsating heat flux. The numerical simulations indicate that the natural convection activity within the enclosure reaches several local maxima for certain values of the heating frequency referred to as resonance frequency.

Finally, it is interesting to underline that the imposition of boundary conditions periodically varies with allocated time, by means of an appropriate choice of the control parameters, to suppress the chaos in some conditions where it normally exists, as reported by Lima and Pettini (1990) and Kim and Stringer (1992), or to establish it were not existing, as reported by Xia *et al.* (1995). These possibilities, offered by variable heating conditions, could be properly exploited according to the application needs.

Sarris *et al.* (2002) numerically investigated natural convection in air-filled rectangular enclosure with sinusoidal temperature profile on the upper wall and adiabatic conditions on the bottom and sidewalls. Results of the study show that, the thermal boundary layer is formed on the upper wall with its thickness decreases while as the Rayleigh number increases. This results in a lower temperature penetration depth and may have important implications in the design of glass melting tanks. Increasing the tank aspect ratio increases the fluid circulation intensity and the thermal penetration depth, which are important parameters for improving glass melt homogenization. Basak *et al.* 2006 performed a numerical study on laminar natural convection in an air-filled square cavity with uniformly and non-uniformly heated bottom wall, and adiabatic top wall maintaining constant temperature of cold vertical walls. The results show that the non-uniform heating exhibits greater heat transfer rates than that with uniform heating for all Rayleigh numbers. Bilgen and Yedder (2007) carried out a numerical study on natural convection of air in rectangular enclosures with sinusoidal temperature profiles on side walls and insulated other ones. The results show that the thermal penetration is a function of the aspect ratio and Rayleigh number. Generally, it approaches to 100% at high Rayleigh numbers when the lower half is heated and the upper half cooled. Results of a numerical study on natural convection in an air-filled rectangular enclosure with linear temperature distributions on both side walls were reported by Sathiyamoorthy *et al.* (2007). Sivasankaran *et al.* 2010 conducted a numerical study on mixed convection in a lid-driven cavity with sinusoidal temperature distribution on side walls, and moving adiabatic top wall. The results show that, when the amplitude of temperature increases, the heat transfer also increases in the natural convection regime. As the velocity of fluid is increases as the Richardson number and amplitude ratio increases too. In another numerical study, Sivasankaran *et al.* (2011) investigated the effects of a magnetic field on mixed convection inside a lid-driven square cavity

with sinusoidal temperature profiles on side walls. They showed that when the left sidewall is kept with sinusoidal temperature distribution, the heat transfer increases and so does the amplitude ratio.

Most of the studies are performed in square enclosures. However, natural convection is very important in other geometries in real life situations, particularly, rectangular enclosures. Wilkes and Churchill 1966 performed a finite difference computation on natural convection in a long horizontal rectangular enclosure. They demonstrated that the steady state results are in good agreement with analytical solutions. The effect of aspect ratio on natural convection of nanofluid was studied by Tong (1999). The results revealed that Nusselt number exhibits a strong dependence on aspect ratio ( $Ar$ ),  $Ra$  and the density distribution of nanoparticles.

In some heat transfer applications, nano-sized particles (average particle size less than 100 nm) are added in the base fluid such as water or ethylene glycol to obtain better thermal properties compared to base flow. Nanofluids have improved heat transfer characteristics with little pressure drop as compared to base fluids (Oztop and Abu-Nada 2008).

The literature review showed that nanofluids lead to improvement in the heat transfer performance, which is in a good agreement with experimental works. Modifications could be made to achieve more accurate results from numerical processes. Shahi *et al.* 2010 have numerically investigated the convective cooling in a square vented cavity and partially heated from below utilizing nanofluids. They showed that increase in solid concentration leads to increase in the average Nusselt number at the heat source surface and decrease in the average bulk temperature.

While applying nanofluids for commercial cooling, Tzeng *et al.* 2005 studied the effect of nanofluids when used as engine coolants. CuO (4.4% wt) and Al<sub>2</sub>O<sub>3</sub> (4.4% wt) nanoparticles and antifoam were individually mixed with automatic oil transmission. The experimental platform was a real-time four-wheel-drive (4WD) transmission system. The experimental results showed that, under similar conditions, antifoam-oil provided the highest temperature distribution in rotary blade coupling and, accordingly, the worst heat transfer effect, and CuO-oil provided the lowest temperature distribution both at high and low rotating speed and, accordingly, the best heat transfer effect. Gosselin and Silva 2004 explored the optimization of particle fraction for maximizing the thermal performance of nanofluid flows under appropriate constraints. They argued that when few particles are present, the achieved heat transfer rate is small, whereas too many particles lead to large shear stresses and large required pumping power. This competition reveals a trade-off opportunity to maximize the heat transfer rate at constant pumping power by selecting the appropriate amount of particles. Using nanofluids as coolants, Chein and Huang (2005) numerically considered silicon microchannel heat sink

performance. The nanofluid was a mixture of pure water and nanoscale Cu particles at various volume fractions. Due to the increased thermal conductivity and thermal dispersion effects, they found that performance was greatly improved when nanofluids were used as a coolant. In addition, they observed that the presence of nanoparticles in the fluid did not produce any extra pressure drop because of small particle size and low particle volume fraction.

**2. STATEMENT OF THE PROBLEM**

The geometry of the studied problem is shown in Fig. 1. It consists of a two-dimensional cavity with height H and length L filled with mixture of water and solid particles CuO. The left wall of the enclosure is heated with a temperature varying sinusoidally in time ( $T_c+a.\sin(\pi t/\Theta)$ ), while the vertical right wall is cooled at a constant temperature  $T_c$ . The horizontal walls are assumed to be insulated and impermeable to mass transfer. The nanofluid in the cavity is supposed to be Newtonian, incompressible and the flow is supposed to be laminar. Thermophysical properties of water and nanoparticle (CuO) are assumed to be constant (table 1). The density of the nanofluid is supposed to be constant except in the buoyancy term where boussinesq approximation is imposed.

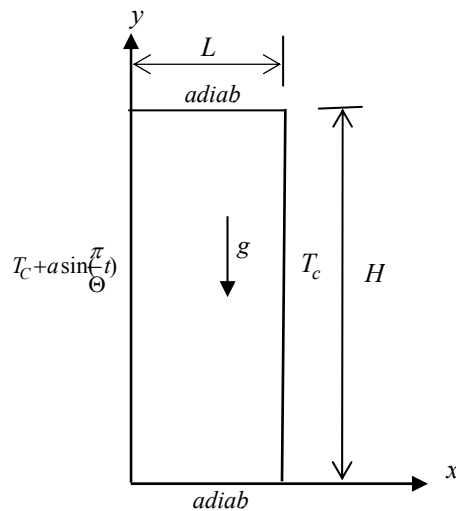


**Fig. 1- Schematic diagram.**

**Table 1 Physical Properties of Pure Water and CuO Solid Particle**

	$\rho$ ( $\text{kg m}^{-3}$ )	$C_p$ ( $\text{Jkg}^{-1} \text{K}^{-1}$ )	$k$ ( $\text{Wm}^{-1} \text{K}^{-1}$ )	$\beta$ ( $\text{k}^{-1}$ )
Pure water	997.1	4179	0.613	$2.1 \times 10^{-4}$
CuO	6320	531.8	76.5	$1.8 \times 10^{-5}$

**3. MATHEMATICAL FORMULATION**

By the law of mass conservation, momentum and energy, the governing equations are:

$$\frac{u}{x} + \frac{v}{y} = 0 \tag{1}$$

$$\frac{u}{\tau} + u \frac{u}{x} + v \frac{u}{y} = -\frac{p}{x} + \frac{\mu_{nf}}{\rho_{nf} \alpha_f} \left( \frac{\partial^2 u}{x^2} + \frac{\partial^2 u}{y^2} \right) + \frac{(\rho\beta)_{nf}}{\rho_{nf} \beta_f} Ra Pr \theta \sin \omega \tag{2}$$

$$\frac{v}{\tau} + v \frac{v}{x} + v \frac{v}{y} = -\frac{p}{y} + \frac{\mu_{nf}}{\rho_{nf} \alpha_f} \left( \frac{\partial^2 v}{x^2} + \frac{\partial^2 v}{y^2} \right) + \frac{(\rho\beta)_{nf}}{\rho_{nf} \beta_f} Ra Pr \theta \cos \omega \tag{3}$$

$$\frac{\theta}{\tau} + u \frac{\theta}{x} + v \frac{\theta}{y} = \frac{\alpha_{nf}}{\alpha_f} \left( \frac{\partial^2 \theta}{x^2} + \frac{\partial^2 \theta}{y^2} \right) \tag{4}$$

The boundary conditions are as follow:

On all solid boundaries:  $u=0 \ v=0$

$$\text{On } x=0, 0 \leq y \leq 1 : \theta = a.\sin(\pi t/\Theta) \tag{5}$$

$$\text{On } x=1, 0 \leq y \leq 1 : \theta = 0$$

$$\text{On } y=0 \text{ and } 1, 0 \leq x \leq 1 : \frac{\partial \theta}{\partial y} = 0$$

The expressions of density, specific heat, thermal expansion coefficient and dynamic viscosity of the nanofluid are given as follows Chein *et al* 2009:

$$\rho_{nf} = (1-\phi)\rho_f + \phi\rho_s \tag{6}$$

$$(\rho C_p)_{nf} = (1-\phi)(\rho C_p)_f + \phi(\rho C_p)_s \tag{7}$$

$$(\rho\beta)_{nf} = (1-\phi)(\rho\beta)_f + \phi(\rho\beta)_s \tag{8}$$

$$\mu_{nf} = \frac{\mu_f}{(1-\phi)^{2.5}} \tag{9}$$

The local Nusselt number  $Nu(x)$  can be expressed as:

$$Nu(y) = -\frac{k_{eff}}{k_f} \left( \frac{\theta}{x} \right)_{x=1} \tag{10}$$

Effective conductivity  $k_{eff}$  of the nanofluid is calculated as follows Koo *et al* 2004:

$$k_{eff} = k_{stat} + k_{brow} \tag{11}$$

The static conductivity  $k_{stat}$  is given by the Maxwell model Maxwell *et al* 1904:

$$k_{stat} = k_f \frac{k_s + 2k_f + 2(k_s - k_f)\phi}{k_s + 2k_f - (k_s - k_f)\phi} \tag{12}$$

The Brownian conductivity is formulated as (Koo and Kleinstreuer 2004):

$$k_{brow} = 5 \times 10^4 \beta(\phi) C_{\beta f} \sqrt{\frac{kT}{\rho_s d_s}} f(T, \phi) \tag{13}$$

Where  $\rho_s$  and  $d_s$  are the density and the diameter of nanoparticles, respectively and  $\kappa$  is the Boltzmann constant  $\kappa = 1.3807 \times 10^{-23} \text{ J / K}$ . For the water-CuO nanofluid, the two modeling functions  $\beta_1$  and  $f$  are experimentally estimated

as :

$$\beta_1 = 0.0011(100\varphi)^{-0.7272} \quad \text{for } \varphi > 1\%$$

$$f(T, \varphi) = (-6.04\varphi + 0.4705)T + (1722.3\varphi - 134.63)$$

for  $1\% \leq \varphi \leq 4\%$ .

The total heat transferred from the hot wall to the flow is evaluated by the space averaged Nusselt number expressed as

$$Nu = \frac{1}{Ar} \int_0^{Ar} Nu(y) dy \quad (14)$$

#### 4. NUMERICAL METHODOLOGY

A modified version of Control Volume Finite-Element Method (CVFEM) of Saabas and Baliga (1994) is adapted to the standard staggered grid in which pressure and velocity components are stored at different points. The SIMPLER algorithm of Patankar 1980 was applied to resolve the pressure-velocity coupling in conjunction with an Alternating Direction Implicit (ADI) scheme for performing the time evolution. The numerical code used here is described and validated in details in Abbassi *et al.* (2001a, 2001b). The conditions necessary to prevent numerical instabilities are determined from a combination of Courant–Friedrichs–Lewy (CFL) conditions and the restrictions on the grid Fourier number. According to the CFL conditions, the distance the fluid travels in one time increment must be less than one space increment ( $\Delta x$  or  $\Delta y$ ), and lead to a constraint on the time step  $\Delta\tau$ :

$$\Delta\tau < \left\{ \frac{\Delta x}{u}, \frac{\Delta y}{v} \right\} \quad (15)$$

From this condition, the used grid and velocity fields, the time step is limited by  $\Delta\tau < 1.57 \times 10^{-4}$ . In the following computations  $\Delta\tau$  is fixed at  $10^{-5}$ .

#### 5. GRID REFINEMENT AND TEST VALIDATION

Grid refinement tests have been performed for four uniform grids:  $51 \times 51$ ,  $61 \times 61$ ,  $71 \times 71$  and  $81 \times 81$  for  $Ra=10^5$ ,  $\varphi=4\%$  and  $Ar=1$  applied to configuration of our problem. Results show that when we moved from the first grid to the second, the Nusselt number ( $Nu$ ) moved from 3.1447 to 3.1185, undergoing a variation of 0.84%. When we moved from the second grid to the third, the Nusselt number becomes 3.1030, undergoing a decrease of 0.50%. Now, when we moved from the third grid to the fourth, the Nusselt number becomes 3.0952, undergoing a decrease of only 0.25%. We conclude that the grid of  $71 \times 71$  is sufficient to carry out the numerical study of this flow. A particular care is taken when varying the aspect ratio; the grid is extended or reduced keeping constant space steps.

The present code was also tested to simulate the case studied by Qi-Hong Deng and Juan-Juan Chang (2008). We calculated the average Nusselt number for the rectangular enclosure with sinusoidal space temperature distributions on the left side wall at  $Pr=0.71$  and for various Rayleigh numbers. As can be seen from Fig 2, the results predicted by current computer code agree well with the previous study.

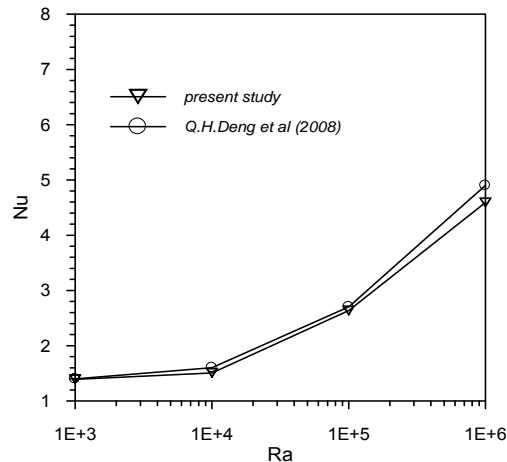


**Fig. 2. Test validation: Comparisons with Qi-Hang Deng and Juan-Juan Chang (2008) with  $Pr=0.71$  and  $Ar=1$ .**

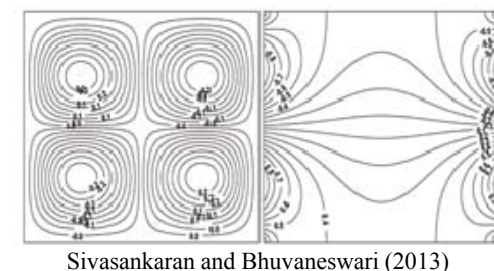
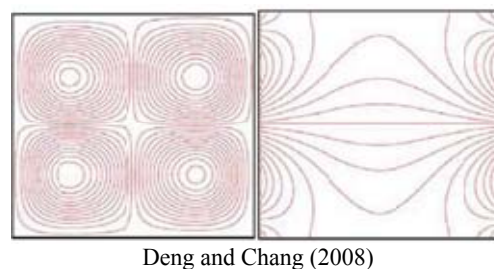
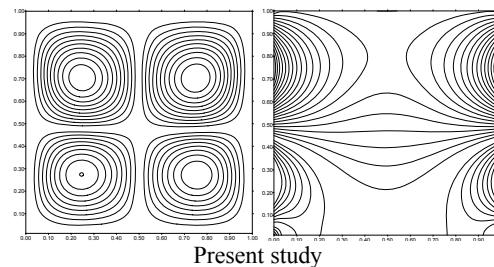


**Fig. 3. Comparison of the present results with Deng and Chang (2008) and Sivasankaran and Bhuvaneshwari (2013).**

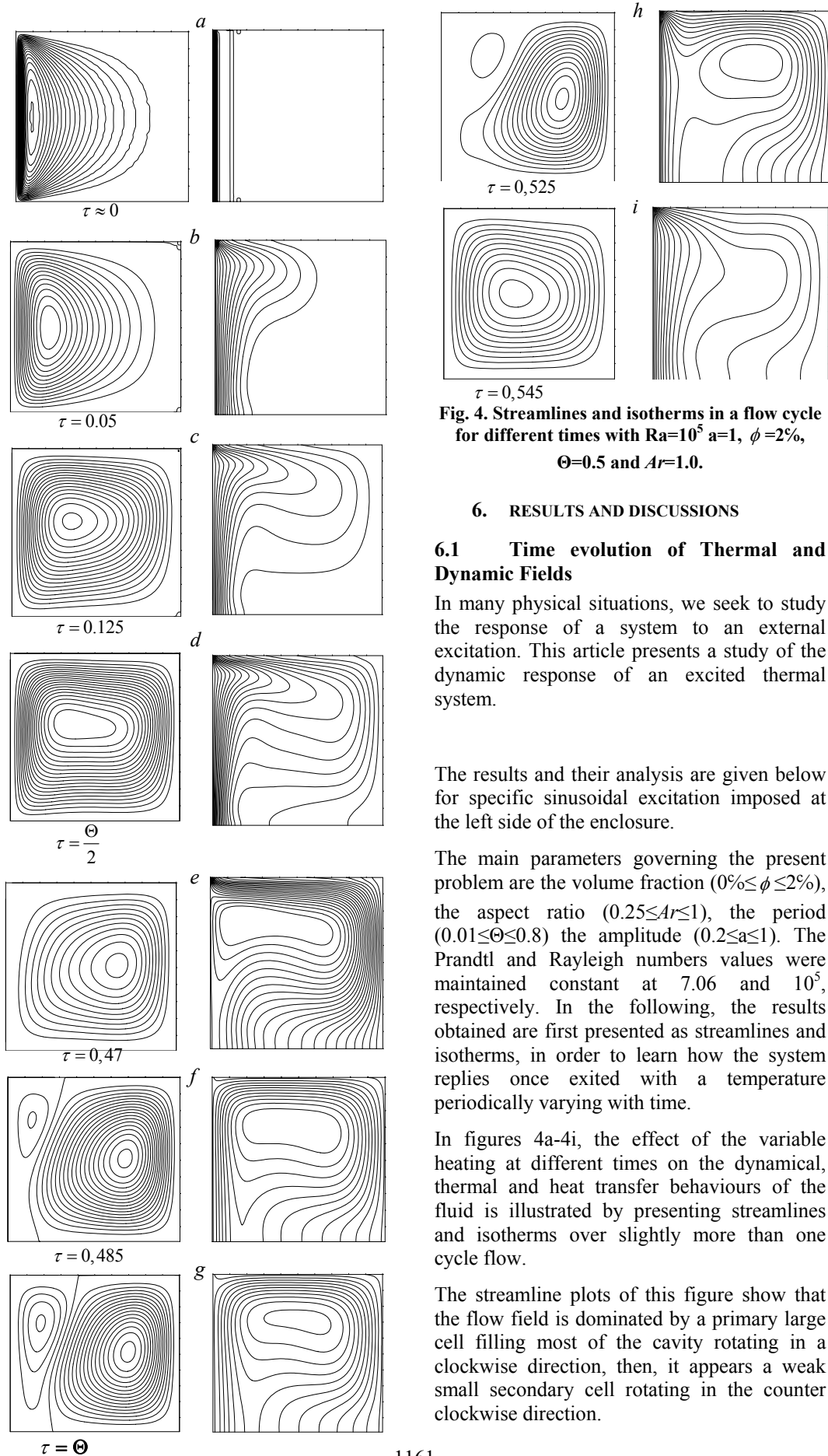


**Fig. 4. Streamlines and isotherms in a flow cycle for different times with  $Ra=10^5$   $a=1$ ,  $\phi=2\%$ ,  $\Theta=0.5$  and  $Ar=1.0$ .**

## 6. RESULTS AND DISCUSSIONS

### 6.1 Time evolution of Thermal and Dynamic Fields

In many physical situations, we seek to study the response of a system to an external excitation. This article presents a study of the dynamic response of an excited thermal system.

The results and their analysis are given below for specific sinusoidal excitation imposed at the left side of the enclosure.

The main parameters governing the present problem are the volume fraction ( $0\% \leq \phi \leq 2\%$ ), the aspect ratio ( $0.25 \leq Ar \leq 1$ ), the period ( $0.01 \leq \Theta \leq 0.8$ ) the amplitude ( $0.2 \leq a \leq 1$ ). The Prandtl and Rayleigh numbers values were maintained constant at 7.06 and  $10^5$ , respectively. In the following, the results obtained are first presented as streamlines and isotherms, in order to learn how the system replies once excited with a temperature periodically varying with time.

In figures 4a-4i, the effect of the variable heating at different times on the dynamical, thermal and heat transfer behaviours of the fluid is illustrated by presenting streamlines and isotherms over slightly more than one cycle flow.

The streamline plots of this figure show that the flow field is dominated by a primary large cell filling most of the cavity rotating in a clockwise direction, then, it appears a weak small secondary cell rotating in the counter clockwise direction.

We note that for the beginning, we observed that the flow main dominant is formed by only one cell rotating in the clockwise sense with an inactive area located close of the right cold wall of the enclosure. The cell centre is positioned toward the hot wall side of the enclosure.

Once the time increases to reach 0.125, the recirculation cell will shift toward to the right. The inactive area is reduced and the flow remains unicellular. At  $\tau=\Theta/2$  the central cell takes an elliptical shape, and the centre of the cell is in the middle of the enclosure.

A secondary cell appears at  $\tau=0.485$  (fig.4(f)) similar to that found by M. kazmierczak et al (1992), this secondary cell grows in size and intensity (Figs. 4(g)) over the second half of the time period of the hot wall temperature variation where the instantaneous hot wall temperature is always less than the average value. Continuing further in time, the region of secondary recirculation greatly decreases in size then totally disappears as  $\tau=0.545$  (Fig. 4(i)).

During the second half of the cycle, simultaneously with the appearance of the secondary flow, the flow intensity in the main cell is much weaker, the maximum stream function  $\psi_{max}$  in the main cell, decreases as time increases ( $\psi_{max}=11.00$  for  $\tau=0.47$  and  $\psi_{max}=7.00$  for  $\tau=0.5$ ) and its location has shifts toward the vertical cold wall.

As regards the isotherms and during the time when the hot wall temperature is increasing (Figs. 4(a)-(d)), a well defined thermal boundary layer is visible on left vertical wall. However, when the hot wall left temperature decreases the thermal boundary layer on the left hot wall moves to the right wall.

**6.2 Heat Transfer Under the Effect of Nanofluid Concentration**

Figure.5 shows the time evolution of the average Nusselt number ( $Nu$ ) for different values of volume fraction, together with the variation of temperature at the left boundary. At the beginning,  $Nu$  is typically zero, indicating that heat does not reach the right wall; therefore the system begins to respond after a finite time delay. After this time the Nusselt number will go up very quickly, it reaches a maximum value and then, gradually decreases. In fact the increase of the volume fraction is accompanied by proportional increase in the amplitude of Nusselt number up to  $\phi=2\%$  and decreases for  $\phi=4\%$  but remains superior to  $\phi=0\%$  (fig.5) similar to

reference Fatih *et al.* (2013). We note that after excitation by a sinusoidal temperature, the response time ( $\tau_{resp}$ ) of the system decreases by increasing the volume fraction of nanoparticles. For  $\phi=0\%$ , the response time  $\tau_{resp}=0.044$ , when  $\phi=2\%$   $\tau_{resp}=0.033$ . For  $\phi=4\%$  the response time increases, but remains below  $0\%$ . We can conclude that the system response time decreases with the increase of volume fraction, indicating that the fluid thermal conductivity becomes more important to the presence of nanoparticles.

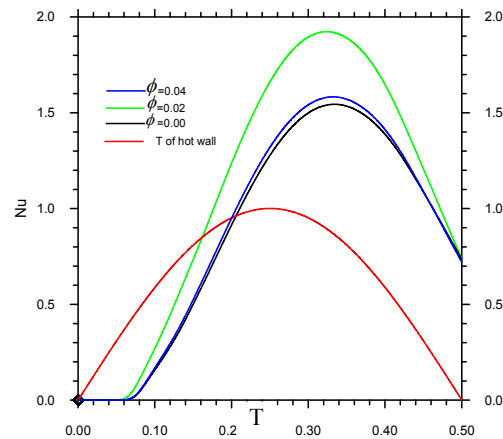


**Fig. 5. Evolution of Nusselt numbers and temperature of the left wall for  $\Theta=0.5$ .**

Table 2 shows the temporal gap between the time of the maximum temperature and the time of maximum Nusselt number, for different volume fraction values. We define by  $\tau_{max}$  the time corresponding to the maximum amplitude, the gap is used to measure the quality of the response. As expected, the addition of solid particles improves the response of system and reduces significantly the time gap.  $\Delta\tau$  decreases remarkably with increasing  $\phi$  reaching a minimum at  $\phi=2\%$  and then increasing slowly but remaining inferior to the case of pure water. The decrease of temporal gap due to solid particle addition up to 2% CuO concentration reaches 17.6%.

**Table 2 Temporal Gap for Different Values of Volume Fraction**

$\phi$	0%	1%	2%	3%	4%
$\tau_{max}$	0.335	0.325	0.320	0.324	0.332
T ( $T_{max}(\text{hot wall})$ )	0.25	0.25	0.25	0.25	0.25
$\Delta\tau=$ ( $\tau_{max}-\tau(T_{max})$ )	0.085	0.075	0.07	0.074	0.082

Figure.6 illustrates the effect of the volume fraction on vertical velocities for pure water as well as the CuO-water nanofluid at the midsection of the enclosure. There is a

difference for velocity profiles between the zero volume fraction and the other volume fractions. This difference is related to adding the nanoparticles into the fluid associated random through the fluid which in turn results in higher velocity for the nanofluid.

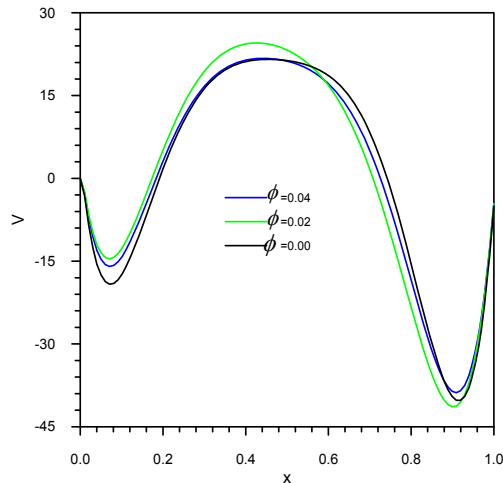


**Fig. 6. Velocity profiles for different concentrations at  $y=0.5$ ,  $Ar=1$ ,  $\tau=0.5$ ,  $a=1$  and  $\Theta=0.5$ .**

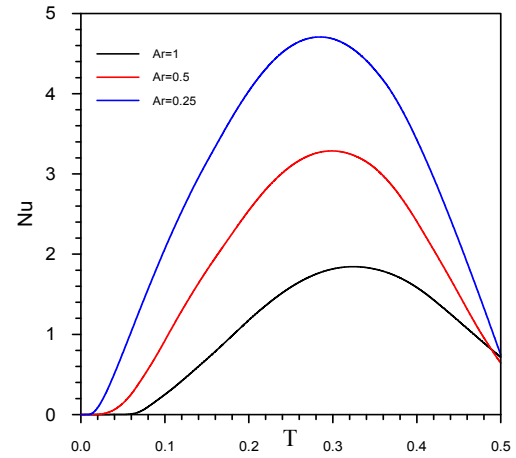
### 6.3 Effect of Aspect Ratio

Figure 7 presented the Nusselt number and their evolutions for different aspect ratios. The results presented put in evidence an obvious effect of aspect ratio ( $Ar$ ) on the amplitude of  $Nu$ . In the range  $0.25 \leq Ar \leq 1$  the amplitude of Nusselt number undergoes a significant increase when  $Ar$  decreases. For all aspect ratio and applied with the heated portion, one periodic excitation temperature, the heat transfer value increases to reach a maximum value and decreases. This value is reached at different times ( $\tau_{max}$ ),  $\tau_{max}$  decreases with decreasing aspect ratio. For  $Ar=1$   $\tau_{max}=0.3247$ ,  $Ar=0.5$   $\tau_{max}=0.2987$  and  $Ar=0.25$   $\tau_{max}=0.2848$ .

We notice that after excitation by a sinusoidal temperature, the response time ( $\tau_{resp}$ ) of the system decreases by decreasing the aspect ratio. For example for  $Ar=1$ ,  $\tau_{resp}=0.033$ , when  $Ar=0.5$ ,  $\tau_{resp}=0.011$ , therefore the system becomes three times quicker than  $Ar=1$ . For  $Ar=0.25$ ,  $\tau_{resp}=0.005$ , the system is seven times quicker compared to  $Ar=1$ . We can conclude that the system response time decreases with the decrease of the aspect ratio, indicating that the speed of fluid flow becomes more important to the aspect ratio decrease.

We also note that after a flow cycle (period) the system does not return to its ground state and this is due to the system inertia that can store the generated energy.

Fig.8 shows the variation of vertical velocity component profiles along the horizontal line passing by the geometrical centre of the enclosure for three aspect ratios  $Ar=1$ ,  $Ar=0.5$  and  $Ar=0.25$ . It is found for a rectangular enclosure that when aspect ratio increases, the fluid velocity increases.



**Fig. 7. Evolution of Nusselt number with time at different values of aspect ratio ( $\phi=2\%$ ),  $a=1$  and  $\Theta=0.5$ .**

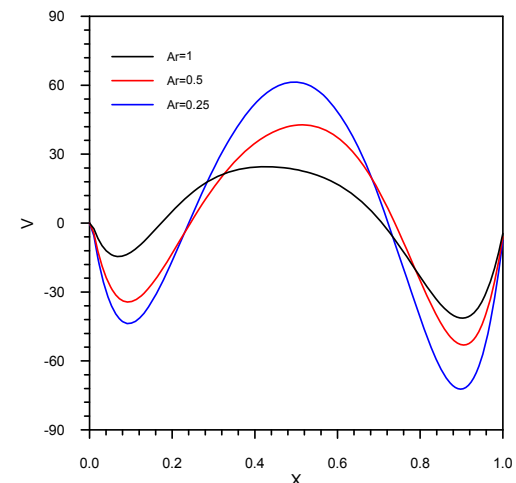


**Fig. 8. Velocity profiles for different aspect ratios at  $y=Ar/2$ ,  $\phi=2\%$   $\tau=0.5$ ,  $a=1$  and  $\Theta=0.5$ .**

### 6.4 Effect of Amplitude and Period

The effect of the amplitude of sinusoidal boundary temperature on the temporal variations of nusselt number  $Nu(\tau)$ , are presented in fig.9. The figure zoom, represents the response of system for different values of amplitude of temperature at the left side wall. The variation of Nusselt number is characterized by increasing amplitudes following the increase of (a). We also note that after excitation the system response time decreases with the amplitude increase, for ( $a=0.2$ ,  $\tau_{resp}=0.0408$ ), ( $a=0.4$ ,  $\tau_{resp}=0.0367$ ),

( $a=0.6, \tau_{resp}=0.0349$ ), ( $a=0.8, \tau_{resp}=0.034$ ), ( $a=1.0, \tau_{resp}=0.0330$ ). We spend from the  $a=0.2$  to  $a=1$ , the decrease of the response times of the system reaches 19%. As for the time of maximum amplitude of  $Nu$ , it decreases with the amplitude increase ( $a$ ).

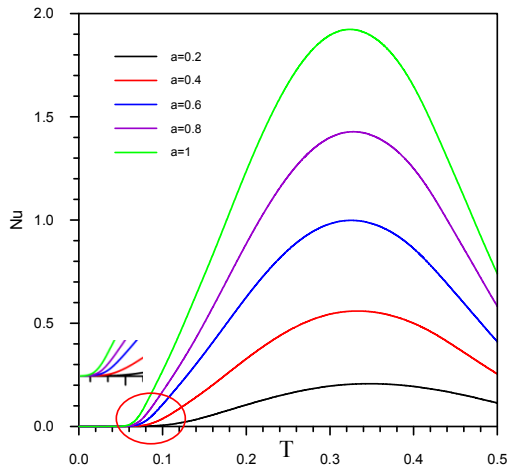


**Fig. 9.** Effect of the amplitude on the variation of Nusselt number in function with time, with  $Ar=1$ ,  $\phi=2\%$  and  $\Theta=0.5$ .

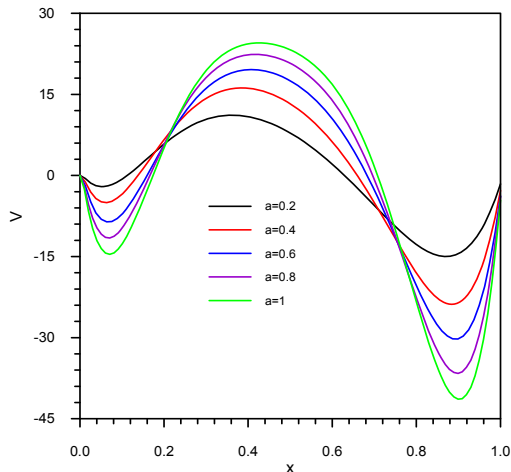


**Fig. 10.** Velocity profiles for different amplitude at  $y=0.5$ ,  $Ar=1$ ,  $\Theta=0.5$  and  $\tau=0.5$ .

Fig.10 illustrates the effect of amplitude ( $a$ ) on the horizontal velocity. There is a significant difference for velocity profile between  $a=0.2$  and  $a=1$ . The velocity is increasing with amplitude ( $a$ ) increasing. We note that in the case where the amplitude of the temperature is equal to 0.2, the Nusselt number at the lower intensity, relative to other amplitude (fig.9) and this is due to the low velocity encountered at this amplitude ( $a=0.2$ ). The effect of the period on the temporal variation of Nusselt number is illustrated in fig.11 for  $a=1$  and different values of  $\Theta$ . In this case, the sinusoidal nature of excitation is relatively well reproduced in the temporal variation of

this quantity  $Nu(\tau)$ . We note that the amplitudes of the oscillations of the Nusselt number increases when  $\Theta$  increases. We can clearly observe that the increase in the period, fact increased the time required for the system response as clearly indicated by the zoom. In fact, in the figure.4 and for various values of  $\tau$ , the important changes in the flow structure are obtained with the low values of the period particularly for  $\Theta=0.5$ . However, when the system is excited with low imposed frequencies, it rapidly replies as shown in the above figure. With increasing the period, heat transfer is enhanced.

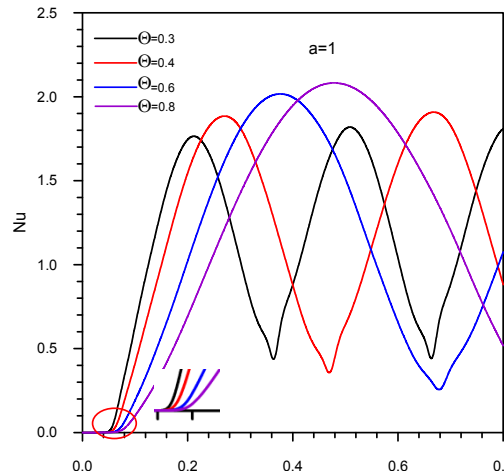


**Fig. 11.** Effect of the period  $\Theta$  in the variation of the Nusselt number in function of time for  $\phi=2\%$  and  $Ar=1$ .

### 6.5 Correlations for Time Response

Figure 12 summarizes the time response variation in function of the amplitude ( $a$ ) and period  $\Theta$ . As can be seen,  $\tau_{resp}$  decreases, as ( $a$ ) increases, but  $\tau_{resp}$  increases with increasing the period. The behavior of this decrease can be modeled by a power law:

$$\tau_{resp} = \alpha \times a^\beta \tag{16}$$

The smoothing by least square method shows that:

$$\alpha = 0.03286 \text{ and } \beta = -0.13033$$

And the increase of  $\tau_{resp}$  as a function of the period is modeled by:

$$\tau_{resp} = \alpha_1 \times \Theta^{\beta_1} \tag{17}$$

The smoothing by least square method shows that:

$$\alpha_1 = 0.03721 \text{ and } \beta_1 = 0.15060$$

Figure 12 shows also that the proposed model agrees well with numerical results, the maximum deviation is less than 3% for  $\tau_{resp}$  as

a function of amplitude, and in the order of 0.27% for  $\tau_{resp}$  as a function of period.

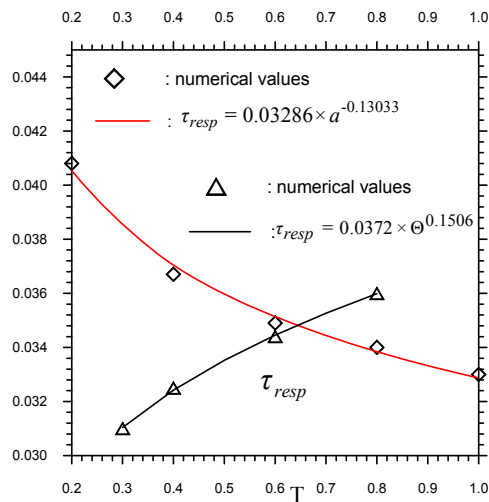


**Fig. 12. Response time as a function of the amplitude and the period of temperature.**

### 7. CONCLUSION

The natural convection in a rectangular enclosure with temporal sinusoidal temperature variation on one side wall has been numerically studied. The coupled non linear equations of momentum and energy including buoyancy forces under the Boussinesq approximation are numerically solved. From the study, the following conclusions are drawn:

1. The system response time decreases by increasing the volume fraction of solid particles.
2. The volume fraction increase is accompanied by proportional increase in the amplitude of Nusselt number.
3. The amplitude of Nusselt number undergoes a significant increase when  $Ar$  decreases.
4. The system responds quickly, when increasing the amplitude of temperature excitation.
5. When the system is excited with low imposed frequencies, it rapidly replies.
6. When the aspect ratio increases, the system response time increases.

### REFERENCES

Abbassi, H. S., S. Turki and B. Nasrallah (2001). Mixed convection in a plane channel with a built-in triangular prism. *Numer. Heat Transfer A* 39(3), 307–320.

Abbassi, H. S., S. Turki and B. Nasrallah (2001). Numerical investigation of forced convection in a plane channel with a built-in triangular prism. *Internat. J. Thermol. Sci.* 40, 649–658.

Antohe, B. V. and J. L. Lage (1996). Amplitude Effect on Convection Induced by Time-Periodic, horizontal Heating. *Int. J. Heat Mass Transfer*. 39, 1121–1133.

Bilgen, W. and R. B. Yedder (2007). Natural convection in enclosure with heating and cooling by sinusoidal temperature profiles on one side. *International Journal of Heat and Mass Transfer* 50, 139–150.

Chein, R. and G. Huang (2005). Analysis of Microchannel Heat Sink Performance Using Nanofluids. *Applied Thermal Engineering*. 25, 3104–3114.

Deng, Q. H. and J. J. Chang (2008). Natural Convection in a Rectangular Enclosure with Sinusoidal Temperature Distributions on Both Side Walls. *Numer. Heat Transfer A* 54, 507–524.

Douamna, S., M. Hasnaoui and B. Abourida (2000). Two-Dimensional Transient Natural Convection in a Repetitive Geometry Submitted to Variable Heating From Below. Numerical Identification of Routes Leading to Chaos. *Numer. Heat Transfer A* 37, 779–799.

Fatih, S. and H. F. Öztop (2013). Identification of forced convection in pulsating flow at a backward facing step with a stationary cylinder subjected to nanofluid. *International Communications in Heat and Mass Transfer* 45 111–121.

Gosselin, L. and A. K. Da Silva (2004). Combined Heat Transfer and Power Dissipation Optimization of Nanofluid Flows. *Applied Physics Letters* 85(18), 4160–4162.

Kazmierczak, M. and Z. chinoda (1992). Compact Buoyancy-driven flow in an enclosure with time periodic boundary conditions. *Int. J. Heat Mass Transfer* 35(6), 1507-1518.

Kim, J. H. and J. Stringer (1992). *Applied Chaos*, Wiley, New York.

Koo, J. and C. Kleinstreuer (2004). A new thermal conductivity model for nanofluids. *J Nanoparticle Res* 6, 577-88.

Lage, J. L. and A. Bejan (1993). The Resonance of Natural Convection in a Horizontal Enclosure Heated Periodically from the Side. *Int. J. Heat Mass Transfer* 36, 2027–2038.

Lima, R. and M. Pettini (1990). Suppression of Chaos by Resonant Parametric Perturbations. *Phys. Rev. A* 41, 726–733.

Maxwell J. (1904). A treatise on electricity and magnetism. 2nd ed. Oxford. Cambridge: University Press 435-41

Oztop, H. F. and E. Abu-Nada (2008). Numerical study of natural convection in partially heated rectangular enclosures filled with nanofluids. *International Journal of Heat and Fluid Flow* 29, 1326–1336.

Patankar, S. V. (1980). *Numerical heat transfer and fluid flow*. Washington, D. C.: Hemisphere Publishing Corporation 113-37.

Roy, T. S. and A. R. Balakrishnan (2006). Effects

- of thermal boundary conditions on natural convection flows within a square cavity. *International Journal of Heat and Mass Transfer* 49, 4525–4535.
- Sivasankaran, S. A. Malleswaran, J. Lee and P. Sundar (2011). Hydro-magnetic combined convection in a lid-driven cavity with sinusoidal boundary conditions on both sidewalls. *International Journal of Heat and Mass Transfer* 54, 512–525.
- Saabas, H. J., and B. R. Baliga (1994). Co-located equal-order control-volume finite-element method for multidimensional, incompressible, fluid flow part I: formulation. *Numer Heat Transf Part B*, 26, 409-24.
- Sarris, I. E., I. Lekakis and N. S. Vlachos (2002). Natural Convection in a 2D enclosure with sinusoidal upper wall temperature. *Numerical Heat Transfer Part A* 42, 513–530.
- Sathiyamoorthy, M., T. Basak, S. Roy and I. Pop (2007). Steady natural convection flows in a square cavity with linearly heated side wall(s). *International Journal of Heat and Mass Transfer* 50, 766–775.
- Shahi, M. A., H. Mahmoudi and F. Talebi (2010). Numerical study of mixed convective cooling in a square cavity ventilated and partially heated from the below utilizing nanofluid. *International Communications in Heat and Mass Transfer* 37 201–213.
- Sivasankaran, S. and M. Bhuvaneshwari (2013). natural convection in a porous cavity with sinusoidal heating on both sidewalls. *Numerical Heat Transfer Part A* 63, 14–30.
- Sivasankaran, S., V. Sivakumar and P. Prakash (2010). Numerical study on mixed convection in a lid-driven cavity with non-uniform heating on both sidewalls. *International Journal of Heat and Mass Transfer* 53, 4304–4315.
- Tong, W. (1999). Aspect ratio effect on natural convection in water near its density maximum temperature. *International Journal of Heat and Fluid Flow* 20, 624–633.
- Tzeng, S. C., C. W. Lin and K. D. Huang (2005). Heat Transfer Enhancement of Nanofluids in Rotary Blade Coupling of Four- Wheel-Drive Vehicles. *Acta Mechanica* 179, 11–23.
- Wilkes, J. O. and S. W. Churchill (1966). The finite-difference computation of natural convection in a rectangular enclosure. *AIChE Journal* 12(1), 161–166.
- Xia, Q. K., T. Yang and D. Mukutmoni (1995). Effect of Imposed Wall Temperature Oscillations on the Stability of Natural Convection in a Square Enclosure. *J. Heat Transfer* 117, 113–120.